A Mechanism of the Penetration Limit for Producing Holes in Poly(4-Vinyl Phenol) Films by Inkjet Etching

ARTICLE *in* JOURNAL OF PHYSICS D APPLIED PHYSICS · SEPTEMBER 2015

Impact Factor: 2.72 · DOI: 10.1088/0022-3727/48/45/455501

3 AUTHORS, INCLUDING:

Yan Zhang

University of Liverpool

7 PUBLICATIONS **14** CITATIONS

SEE PROFILE

David Christopher Whalley

Loughborough University

155 PUBLICATIONS **692** CITATIONS

SEE PROFILE

A mechanism of the penetration limit for producing holes in poly(4-vinyl phenol) films by inkjet etching

Yan Zhang*, Changqing Liu and David C Whalley

Wolfson School of Mechanical and Manufacturing Engineering, Loughborough University, Loughborough, Leicestershire, LE11 3TU, UK

Received 18 June 2015, revised 17 September 2015
Accepted for publication 18 September 2015

Abstract

A penetration limit has been experimentally demonstrated for inkjet etching of holes in thin polymer layers. A mechanism combining the competing coffee ring flow, polymer dissolution and diffusion into the solvent drop, and the interaction between the contact line during evaporation and the softened deformable polymer, is proposed to explain the existence of such a penetration limit. The height-averaged velocity of the coffee ring flow within the evaporating sessile drop is calculated during the initial stage of this etching process when the spherical cap geometry assumption is valid. This is compared with the diffusion velocity of the disentangled polymer into the solvent. The two competing flows are used to elucidate why a hole could be formed initially. The complex wetting dynamics of the receding contact line is included to explain the via hole profile evolution in the later stage of the etching process and the existence of a penetration limit. These two stages are differentiated by the drop volume with respect to the volume of the via hole produced by the preceding drop. The competition between the coffee ring flow transferring polymer away from the central region and the polymer diffusion within the solvent drop is postulated to contribute to either via hole formation or a penetration limit, depending on which one of the two processes is dominant within the solvent evaporation time scale.

Keywords: inkjet etching, polymer patterning, via hole, coffee ring, wetting dynamics

(Some figures may appear in colour only in the online journal)

1. Introduction

Facilitated by the development of various direct-write tech-niques and of functional materials such as polymer-based conductors and semiconductors, printed electronics are flourishing both commercially and as a research topic. This is not only because of simpler manufacturing routes and lower costs, but also as a result of lower processing temperatures and better compatibility with flexible substrates, along with other breakthroughs such as low temperature and nanocomposite inks developed [1, 2], compared with their conventional coun-terparts. Inkjet printing, as one of the numerous direct-write techniques, has been receiving great attention over the past decade due to its merits such as being noncontact, maskless, and compatible with flexible substrates along with consuming less materials. It has been utilized to print functional components such as strain sensors [3], RF power amplifiers [4], magnetic cores [5], supercapacitors [6], conductive tracks [7], transistors [8, 9] and OLEDs [10] in electronics applications. The development of conventional electronics has been guided by Moore's Law, the driver for which lies in the demand for electronic devices with better performance and portability at lower prices. Therefore, one can expect a similar trend for printed electronics to guide its development. Multi-layered printing could be adopted in printed electronics to achieve higher density integration, so that this development trend can be maintained. In such circumstances, the creation of vertical interconnections in printed electronics will be required in the future when scaling and system integration are necessary to further reduce costs and improve performance.

Inkjet deposition of materials may however lead to inhomogeneous deposition due to the coffee ring effect. This effect, also known as the coffee stain effect, exists as a commonly observed phenomenon where drying of a sessile drop results in

*Current address: Center of Materials and Structures, School of Engineering, Univeristy of Liverpool, The Quadrangle, Brownlow Hill, Liverpool, UK, L69 3GH. Email: Yan.Zhang3@liverpool.ac.uk

material suspended or dissolved in the liquid being deposited as a ring. The occurrence of the coffee ring effect is generally unfavourable for printing of functional materials, such as for conductive tracks, as the inhomogeneous material deposition inhibits the conductivity of the structure [11]. Interestingly however, several investigations of deliberately utilizing the coffee ring effect as a means of generating structural patterns in various polymers have also been reported [12–16]. These polymer patterning investigations can be potentially useful in some structural or functional applications. Bonaccurso *et al* [17] and Pericet-Camara *et al* [18] used inkjet printing to fabricate microvessels and microlenses while Xia *et al* [19, 20] and Lu *et al* [21] demonstrated using the same technique to create cavities for display applications.

One potential application of this patterning technique is dissolving via holes in dielectric layers to allow creation of vertical connections between layers in printed electronics. Inkjet etching of via holes can provide good integration with other inkjet-printed features simply by switching firing nozzles. This is of particular interest as it facilitates all-inkjet-printing by providing a subtractive manufacturing means. Using inkjet printing as an etching tool for producing via holes was first demonstrated by Kawase *et al* [8, 22, 23]. Kawase *et al* successfully demonstrated all-polymer thin film transistor circuits, with the via holes used for the vertical interconnection structures made by inkjet etching utilizing the coffee ring effect. Lennon *et al* [24] also used inkjet printing as an etching method to create openings in inorganic SiO_2 layers for solar cell applications. A process of using a single resist layer for multiple patterning steps was also reported [25]. Both applications demonstrated by Lennon used dissolution of a polymer layer to form an intermediate patterning mask rather than the final product. Yang *et al* [26, 27] used inkjet printing to dispense a silver particle loaded ink onto a polymethylmethacrylate (PMMA) surface so that the silver particles were embedded into the dielectric layer as a result of polymer swelling and dissolution to create an electrically conductive path between layers. Even though it has been more than a decade since inkjet etching was first used to dissolve via holes for applications in electronics, it is still an underdeveloped method and more systematic investigations are needed to allow a detailed understanding of the underlying physics and chemistry. Previous work has identified the factors which influence the size of the inkjet-etched via holes and the penetration of the polymer layer [28, 29]. It is postulated that using such a technique to fabricate via holes can only achieve a certain aspect ratio, i.e. ratio of hole diameter to film thickness. This paper aims to demonstrate experimentally a penetration limit and to provide a mechanism to explain why such a limit exists instead of it being possible to excavate the polymer layer completely as the polymer layer thickness increases. This study is of essential importance for the evaluation of inkjet etching of via holes before it can ultimately find suitable applications.

2. Materials and methods

Acetone (CHROMASOLV®, for HPLC, ⩾99.8%, Sigma-Aldrich UK) and Decon 90 (Fisher Scientific UK) were used to clean glass substrates before spin coating them with a thin film of polymer. Poly(4-vinyl phenol) (PVPh) (molecular weight M_w 11 000, ⩽0.2% wt% monomer, density 1.16 g ml^{-1}, glass transition temperature T_g 130–185 °C, Sigma-Aldrich UK) was used as the dielectric polymer and dissolved into IPA (isopropyl alcohol) (Sigma-Aldrich UK) using an ultrasonic bath to produce a clear solution, which was subsequently spin coated on the cleaned glass substrates. Various PVPh thicknesses were achieved by varying the concentration of the polymer solution and the spin coating parameters. A much thicker crack-free polymer layer was used to demonstrate the penetration limit using poly (acrylic acid) (molecular weight M_w 100 000, 35 wt% in H_2O, 1.14 g ml^{-1}, Sigma-Aldrich UK). A CLA (chromatic length aberration) gauge with a vertical resolution of 10 nm was utilized to measure the polymer film thicknesses. IPA was also used as the etchant and was dispensed using a Microfab Jetlab® 4 inkjet printer onto the PVPh coated glass. A WLI (white light interferometry) microscope was used to scan the topography of the holes produced.

When the voltage changes in a waveform, it first generates two negative pressure waves heading towards the reser-voir and the orifice at both ends of the channel, which fills it with ink from the reservoir and retracts the meniscus. The negative pressure wave bounced back from the orifice conserves its phase while the one reflected from the reservoir inverts into a positive pressure wave. The voltage plateau is essential to allow these two reflected waves to travel to the piezoelectric actuator before a positive wave is generated by the actuator following a further voltage change to cancel the reflected negative pressure wave and reinforce the reflected positive pressure wave. This inverts the meniscus outward to eject a drop. The travelling wave inside the channel of the print head and the consequent meniscus oscillation are believed to be the principle of drop formation during inkjet printing [30, 31]. Waveform parameters need to be optimized for the material being printed so that the generated drops have no satellite drops or trajectory deviation. Satellite drops are formed from the tail thread occurring behind the main drop when an excessive amount of solvent is jetted out of the inkjet nozzle, as shown in figures 1(a) and (b). The tail thread can either forward-merge into the main drop, as demonstrated in figure 1(a), or back-merge into one or several satellite drops, as shown in figure 1(b), or could become infinite satellites which travel at the same speed as the main drop without merging [32]. Satellite droplets can lead to variation in the total amount of solvent jetted out for each dispensing event and cause issues of trajectory deviation and therefore poor landing location repeatability, as shown in figure 1(a), accordingly resulting in bad via hole formation. Figure 1(c) illustrates an example of IPA drop formation ideal for via hole production. The drop trajectory is perpendicular to the substrate and no satellite drops are formed.

The diameter and volume of the jetted IPA droplets were analysed using the drop analysis function integrated within the printing system. A more trusted method for drop volume and diameter estimation was performed by weighing a large number of non-volatile ethylene glycol droplets collected in a vial to acquire the uncertainty of this estimation. The

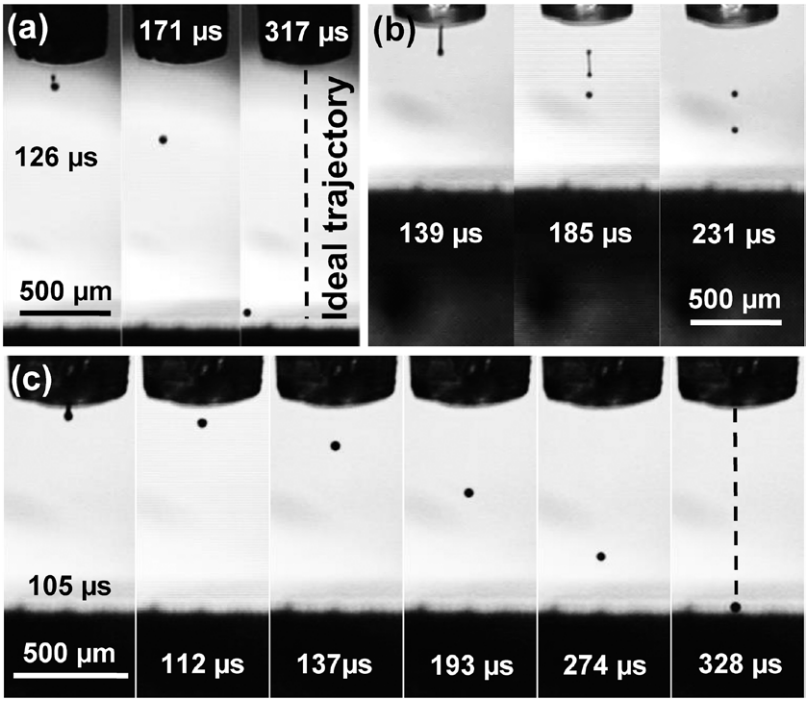

Figure 1. (a) Drop formation featuring a satellite drop forward-merging into the main drop and its deviation from the ideal trajectory; (b) drop formation featuring a main drop with two satellite drops merging into one as they traverse the nozzle–substrate distance; (c) an ideal drop formation for inkjet etching of via holes without satellite drops or trajectory deviation from being perpendicular to the stage.

discrepancy between these two estimation methods is roughly 4.6%. The uncertainty in the weighing method as indicated by the resolution of the weighing scale used is of the order of 2.0%, which implies an overestimation of the drop diameter by $4.6 \pm 2.0\%$ using the drop analysis in Jetlab 4. Therefore this does not significantly affect the results here. Once the waveform was optimized for the etchant, the drop analysis was performed 10 times and the diameter was estimated to be 38 ± 2 μm. The ejection frequency of jetting the IPA drops was set to 1Hz, which gives a 1s time interval between two consecutive drop jets. The evaporation time of an IPA sessile droplet is estimated to be approximately 0.6 s using the Schönfeld model [33]. Therefore in these experiments the drops are believed to have evaporated almost entirely before the next one arrives. A script was written to define the number of drops to be dispensed at each location. After several drops, the PVPh layer is completely etched through, resulting in a crater-like hole. The complete removal of polymer from the bottom of such via holes has been confirmed previously using an electroplating technique [28].

3. Results

The first drop problem is a well-known issue in inkjet printing and is the inconsistency of the first few drops ejected by a nozzle after it has been sitting idle for some time and is caused by evaporation of the ink at the orifice [34]. This evaporation shifts the physical and chemical properties of the ink away from those required and causes problems with proper jetting, especially after prolonged idle times. The time that an ink can successfully wait in an orifice without jetting, termed as the ink latency, varies from a few seconds to a few minutes in commercial drop-on-demand inkjet printers [35], so the frequency of 1 Hz used throughout this work corresponded to a smaller idle time. Additionally the fact that the ink loaded in the reservoir is pure solvent, rather than one of the usual sol inks containing suspensions of particles, means that evaporation will not alter its properties. Therefore the ejection frequency of 1 Hz was not seen to sabotage the hole formation in terms of location repeatability and the resulting via hole dimensions. Figure 2 demonstrates optical microscopy images of via holes produced by various numbers of drops and the superimposition of their profiles. The fact that the outer diameter of the via hole produced by a single drop is approximately the same with that of the hole produced by 5, 20 and 40 drops confirms this. Experiments were carried out several times and could be repeatedly reproduced as long as the initial jetting was established properly.

The inner diameter (D_{in}), outer diameter (D_{out}), ridge height (H_r) and hole depth (H_d) are defined as in the inset in figure 3(a). D_{out} remains independent of N_d at the drop ejection frequency used as shown in figure 3(a). D_{in} has been previously shown to decrease initially with the number of drops (N_d) and then stay constant regardless of N_d, once complete penetration has been achieved, when the jetting frequency allows for substantial solvent evaporation [28]. 7–10 drops are usually needed for complete penetration, depending on polymer thickness, drop diameters, etc. D_{in} versus N_d ($N_d \geqslant 20$) is plotted in figure 3(b) where it can be seen that the average equilibrium D_{in} decreases with increasing polymer thickness. The average equilibrium D_{out} and D_{in} are plotted against polymer thickness in figure 4. Due to the resolution limit of the

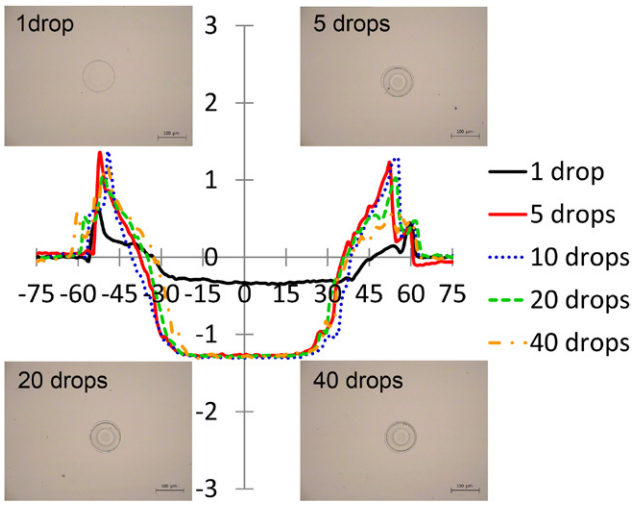

Figure 2. Profile superimposition for holes together with inset optical microscopy photos (scale bar 100 μm) of holes produced by 1, 5, 10, 20 and 40 IPA drops.

inkjet printer and the difficulty of further increasing the thickness of spin coated PVPh without cracking, the penetration limit was not obtained experimentally for PVPh. However, extrapolating from figure 4 implies there should be a thickness limit above which a droplet of a specific volume cannot completely etch through the entire polymer layer. A different polymer, PVA, was therefore used to demonstrate that polymer residue cannot be removed from the bottom of via holes completely above a certain thickness, and the results from this experiments are plotted in figure 5. The PVA polymer thickness was approximately 6.1 μm. D_{out} remained constant with N_{d}, as illustrated in figure 5, while D_{in} is not sketched as the profile quickly shifts to a more concave shape and prevents D_{in} from being determined clearly. However it can be seen that H_d remains far below the polymer thickness (H_0) even at $N_{\text{d}} = 50$, which implies incomplete penetration.

The fact that PVPh films up to 5 μm thick can be etched completely seemingly makes the case less important, as thicknesses of this order maybe too thick for typical printed electronics applications. Nonetheless there are technologies to further reduce inkjet nozzle sizes and thereby to bring the drop size down to a few microns, while printed transistors with channel feature sizes of several microns or even sub-micron have already been demonstrated [36–42]. Droplets of a smaller diameter generated with a high-resolution inkjet printer will undoubtedly diminish the maximum penetration thickness far below 5 μm and will therefore make this issue relevant to printed electronics applications. We propose in the following sections a mechanism to explain why such a hole feature could be form in the polymer layer initially, and a penetration limit exists eventually instead of it being possible to keep dissolving polymer from the hole bottom and thereby increase the aspect ratio.

4. The coffee ring flow and polymer diffusion

In the coffee stain effect, suspended particles accumulate at the border of the sessile drop as a result of outward flow within the evaporating drop induced by the greater rate of

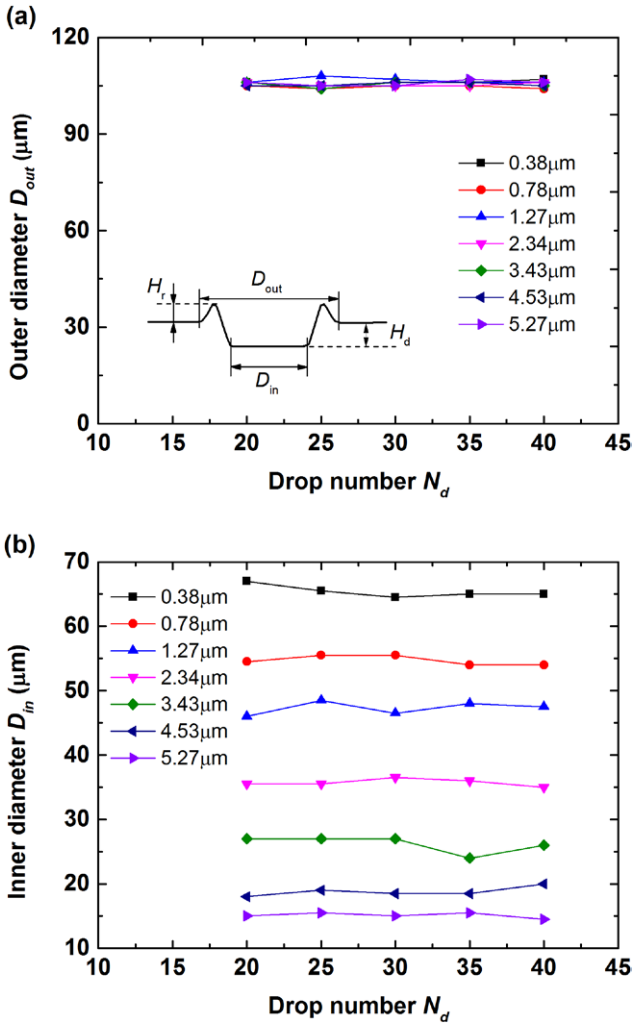

Figure 3. (a) Outer diameter (D_{out}) and (b) inner diameter (D_{in}) versus the number of drops (N_{d}) dispensed for different polymer thicknesses.

evaporation from the edge and a pinned contact line between liquid and solid substrate due to the roughness or chemical heterogeneity of the substrate [43–45]. There are two principal evaporating modes for a sessile drop, known as the constant contact angle mode and the constant contact area mode. The constant contact angle mode is an evaporation process where the contact line recedes as the volume drops while the contact angle remains constant, while the constant contact area mode is an evaporation process where the contact line is pinned and the contact angle therefore decreases as the volume reduces.

In this study it is assumed that PVPh does not dissolve into the IPA drop during the initial impact and spreading phrase, which is supported by the estimation of the time scales associated with each process later. The initial contact angle can therefore be calculated from the drop volume and maximum wetting diameter based on a spherical cap geometry. This geometry assumption holds true when the bond number $Bo = \rho g D^2/\sigma$ (where D is the drop diameter, ρ is the density, g is the gravitational acceleration and is σ the kinematic viscosity) is small ($Bo \ll 1$) [46]. Based on this spherical cap assumption and geometry relationships, the initial contact

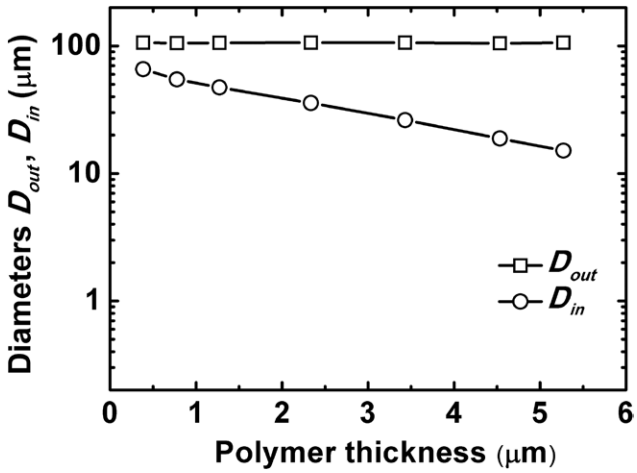

Figure 4. The relationship between outer diameter (D_{out}) and inner diameter (D_{in}) of completely etched holes and polymer thickness.

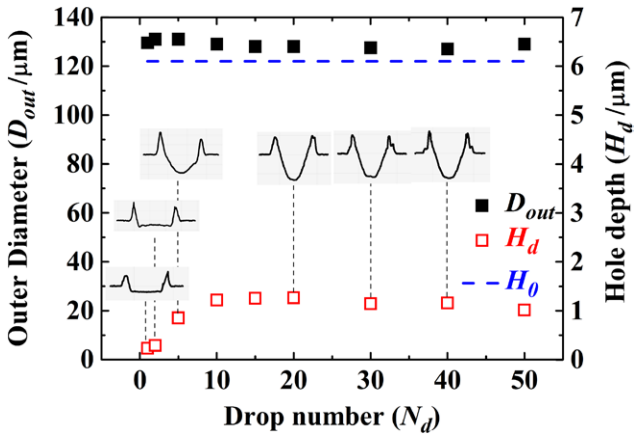

Figure 5. Profile evolution with N_{d} for holes produced in poly (acrylic acid) with deionized water (profiles are not sketched to scale).

angle for the IPA sessile drops on the PVPh layer was calculated to be approximately 14° with a known contact diameter (equivalent to D_{out}) and drop volume. Figure 6 shows a cross section of an evaporating drop and defines the cylindrical coordinate system used to derive an expression for the outward velocity caused by the coffee ring effect assuming a height-averaged coffee ring flow as a function of radius.

Using this coordinate system, the vertically averaged outward radial flow of the liquid $v(r,t)$ caused by the coffee ring effect can be expressed as [45]:

$$v(r,t) = -\frac{1}{\rho r h}\int_0^r \left[J(r,t)\sqrt{1+\left(\frac{\partial h}{\partial r}\right)^2} + \rho\frac{\partial h}{\partial t}\right] r\mathrm{d}r, \quad (1)$$

where $v(r,t)$ is the averaged radial flow of the liquid (m s^{-1}); R is the wetting radius of the sessile drop on the substrate (m); θ is the contact angle (rad);ρ is the density of the liquid (kg m^{-3}); h is the height of the sessile drop at radius r (m); and $J(r,t)$ is the mass loss from the sessile drop per unit area per unit time (kg m^{-2} s^{-1}).

Equation (1) can be expressed as (2) following the detailed derivation described in the appendix:

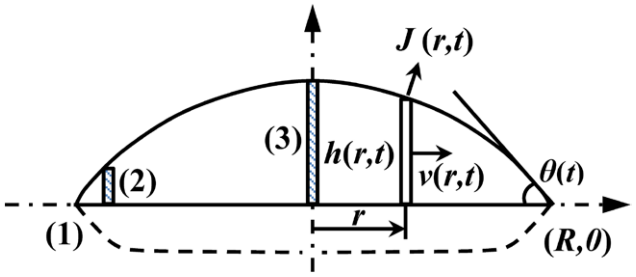

Figure 6. Cross section of an evaporating sessile drop in a cylindrical coordinate system with relevant parameters: evaporation flux $J(r,t)$, fluid velocity $v(r,t)$, contact angle $\theta(t)$, drop height $h(r,t)$ and maximum wetting radius R.

$$\begin{aligned} v(r,t) &= v(r,\theta) \\ &= -\frac{RDc_v(0.27\theta^2+1.30)}{2\rho r\sqrt{\frac{R^2}{\sin^2\theta}-r^2}-\frac{R}{\tan\theta}}\left[\left(1-\frac{r^2}{R^2}\right)^{0.6381-0.2239\left(\theta-\frac{\pi}{4}\right)^2}-1\right] \\ &\quad -\frac{RDc_v(0.27\theta^2+1.30)}{2\rho r\sqrt{\frac{R^2}{\sin^2\theta}-r^2}-\frac{R}{\tan\theta}}\left[\left(1-\frac{r^2}{R^2}\right)^2-1\right]. \end{aligned} \quad (2)$$

The diffusion coefficient of IPA in air, D, can be calculated with the formula in the literature [47] to be $D \approx 9.96\times10^{-7}$ m^2 s^{-1}; $R = D_{\text{out}}/2 = 53$ μm; $c_v = 1.046\times10^{-7}$ g m^{-3}; $\rho = 786$ kg m^{-3}. The outward coffee ring flow velocities at different contact angles within the sessile drop can now be calculated and are sketched as a function of radial location and contact angle in figure 7.

The diffusion rate of polymer into the solvent can be calculated by (please refer to the appendix for details):

$$v_{\text{d}} = \mathrm{d}L/\mathrm{d}t = \sqrt{k_{\text{B}}T/(\sqrt{6n}\,\pi\mu l t)}. \quad (3)$$

The viscosity of the solvent drop is taken to be that of the pure solvent and the temperature gradient within the droplet is neglected to simplify the scenario, while l is taken to be the C–C bond length, 0.154 nm [48]. The diffusion velocity now can be approximated by $v_{\text{d}} \approx \sqrt{178/t}$ μm s^{-1}. According to Hu and Larson, the decreasing rate of the drop height is nearly constant during evaporation [49]. This gives $\dot{h}(0,\tilde{t}) \approx -h_0/t_{\text{e}}$, where $\dot{h}(0,\tilde{t})$ is the drop height reduction rate, h_0 is the initial drop height and t_{e} is the drop evaporation time. The drop height $h(t)$ at any time t can therefore be estimated as $h(t) \approx h_0 - (h_0/t_{\text{e}})t$. The drop height $h(r,t)$ can be expressed as $h(r,t) = \sqrt{R^2/(\sin\theta)^2 - r^2} - R/\tan\theta$, based on the spherical cap geometry. Now the contact angle can be correlated with time so that the diffusion velocity can be sketched along with the coffee ring flow in the same diagram as illustrated in figure 7.

It should be noted here that the infinite diffusion velocity singularity at $t = 0$ (corresponding to an initial contact angle $\theta = 14°$) is not sketched in figure 7. The singularity at the contact line occurs due to the evaporation flux singularity there when using $J(r,t) = J_0(\theta)(1-\tilde{r}^2)^{-\lambda(\theta)}$. In addition, the actual polymer diffusion velocities would be smaller than as sketched at the corresponding contact angle in figure 7 as the

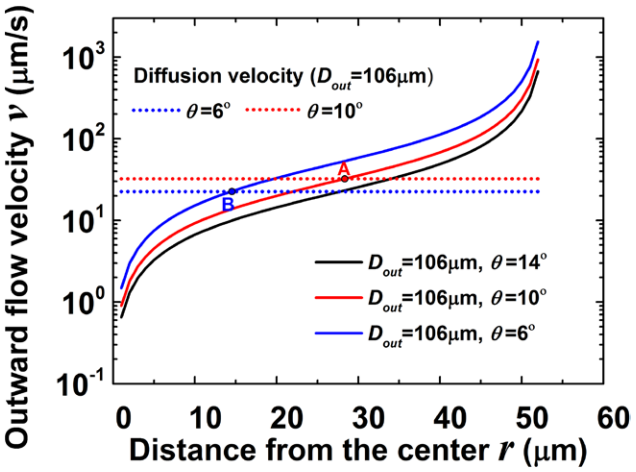

Figure 7. Plot of the outward flow velocity and the inward diffusion velocity as a function of distance from the centre at different contact angles (i.e. times) within the sessile drop.

viscosity increases with ongoing evaporation significantly. However, the coffee ring velocity curve shifts upward and the diffusion velocity line shifts downward as the contact angle decreases with ongoing evaporation, implying an increasing outward coffee ring flow and decreasing polymer diffusion with evaporation. When the contact angle $\theta = 10°$, the coffee ring flow is equal to the diffusion flow at point A, as sketched in figure 7. When the contact angle decreases to $\theta = 6°$, the location at which these two flows are equal shifts to *B*, suggesting more regions within the hole are influenced more strongly by the coffee ring flow. It is therefore concluded that during the initial stage the coffee ring flow will be dominant while the spherical cap shape assumption is valid. Therefore for the first few drops, when the solvent can still be assumed to have a spherical cap shape, at least in the central region of the via hole, within the evaporation time scale of the sessile drop t_e, it is likely that $h\,(r, t) \gg L$. It should be noted that the profiles of the via holes are not shown to scale and they actually have large diameters with respect to their very shallow depths. Therefore horizontal etching of the sidewall can be neglected compared with the vertical downward etching when considering the central region away from the contact line in the early stages. The coffee ring flow transfers the dissolved polymer outwards so that the process is flow dominant [15] and more polymer can be dissolved each time a new droplet is dispensed and transferred outwards to the periphery. This contributes to the initial increase of the via hole depth with an increasing N_d.

The issue with using a height-averaged flow lies in the fact that the radial coffee ring flow velocity changes with height. The coffee ring flow has been shown using mathematical models to be strong along the liquid–gas interface and gradually become weaker nearer the liquid–substrate interface [50]. Additionally the viscosity of the drop may decrease from the contact line to the centre in practice, causing a decreasing diffusion velocity gradient accordingly. This explanation given above in this section may only be a reasonable approximation when the etching depth is small, so that the polymer dissolution and topography do not affect the sessile drop shape significantly and the models of the sessile drop evaporation adopted still apply. As the etching depth increases, the spherical cap assumption is not valid anymore and the wetting conditions change significantly, which will be discussed in the following section.

5. Effect of wetting dynamics

The molar mass of the PVPh used here at 11 000 g mol^{-1}, is less than half of the reported entanglement molar mass, 29 300 g mol^{-1}, for this polymer [51]. Therefore the dissolution rate of PVPh into the solvent, i.e. polymer disentanglement rate, is faster than the diffusion rate of solvent into the polymer, i.e. polymer swelling rate. That is to say the glassy state PVPh can absorb just a small fraction of solvent before converting into the solid swollen glassy state or the viscoelastic rubber-like state and then quickly disentangles and disperses into the solvent. The effect of the solid non-deformable substrate strongly affects the deformation of the elastomer film by the capillary pressure when the polymer layer is thin [52]. As a result, it is reasonable to believe that thin polymer layers are easier to penetrate than thick ones since the pattern profile deformed in thick polymer approaches a predicted parabolic curve [52, 53]. Nonetheless the thickness range of the polymer layers used here is postulated to fall within the thin polymer category in the work by Pericet-Camara *et al* [52]. However, both solvent evaporation and polymer dissolution are involved and cannot be neglected in our work. In addition, multiple drops are dispensed at the same location, which makes the situation far more dynamic and complex.

Let us therefore now consider the situation when only one drop is dispensed on the polymer layer. The timescale for drop impact, i.e. the time for a drop to spread from the moment of impact until when the maximum spreading is achieved, can be estimated by $t_c = 8D_0/3v$ (where D_0 is the drop diameter and v is the impact velocity) [54]. For a Φ40–50 μm IPA drop with impact velocities of 1–3 m/s, t_c is estimated to be 0.04–0.13 ms, which is in agreement with the timescale of the significant stages of a Φ40–50 μm drop impact and sessile drop formation reported to be 0.1 ms by Dong *et al* [34]. The polymer dissolution process is taken to be of a similar timescale as solvent absorption into the polymer, which happens in a few milliseconds [55]. The estimated evaporation time of an IPA drop has already been calculated to be approximately 0.6 s. Therefore it is postulated that the droplet first lands on the substrate and spreads out into a sessile drop in the shape of a spherical cap with a negligible gravitational effect when the bond number *Bo* is small. When quasi-equilibrium is achieved, the three phase contact line attains its maximum spreading diameter. Polymer dissolution and solvent evaporation occur subsequently, with evaporation being the longest process. It should be noted that estimation of the evaporation time for a sessile drop by the Schönfeld model is used here for a qualitative purpose only due to the lack of mathematical models for soluble substrates. However, if the evaporation time of the drop on soluble substrates were comparable to drop spreading, it is unlikely a hole will be created due to

the lack of time for the coffee ring effect to transfer the dissolved polymer outwards or the Laplace pressure to deform the softened region. Consequently, it is still sensible to believe that the evaporation process is the longest even though there is a potentially large error in estimating the evaporation time of the drop caused by the dissolution of the polymer.

If we look at three radial locations within the sessile drop with one at the contact line, one 5 μm away from the contact line, and another one at the centre, as indicated by (1), (2) and (3) in figure 6, the initial heights at three locations when the sessile drop is in quasi-equilibrium with the polymer layer are calculated to be approximately 0 μm, 1.2 μm and 6.5 μm respectively. If we assume the diffusion is 1D and only along the vertical axis when polymer dissolution occurs, the quantity of solvent available for the PVPh to dissolve into is lower near the contact line compared with in the centre. In addition, the faster evaporation rate at the contact line also means that the polymer concentration will more easily saturate there than nearer to the centre. Accordingly the etching depth near the contact line can be expected to be smaller than that in the interior of the sessile drop. Studies have already shown that solvent ingress into the polymer generates various layers in the bulk polymer [56]. It is therefore believed that in this situation a solid swollen region, as indicated in figure 8(a), exists below the etched depth and above the unaffected glassy polymer due to the solvent diffusion into PVPh and the inhibition of continuous polymer ingress into the solvent caused by a lower diffusion rate resulting from a viscosity increase. Since the disentanglement rate is high, a much lower Young's modulus can be expected in this region even with just a small fraction of solvent penetration. In the rubber-like region where polymer chains disentangle into the pure solvent, it is postulated that the capillary pressure ΔP hardly plays any role since the drop is in equilibrium of a hydrostatic state. Nonetheless since the swollen polymer is in the glassy state in the solid swollen region, the capillary pressure is believed to be behind the deformation of the softened polymer [57]. It has been demonstrated that this deformation results in a parabolic dimple for thick polymer layers but that if a rigid non-deformable substrate lies below a thin film this substrate shifts the parabolic profile to a more flat or even convex bottom [52, 53, 58, 59]. Based on experimental results and the above analysis, the via hole sidewall usually has a small leaning angle with the bottom. Due to the upward pulling effect of the vertical component of the liquid surface tension, the three phase contact line is deformed and the wetting condition changes from that shown in figure 8(a) to the situation shown in figure 8(b) where there is a sudden increase of the contact angle (θ_1) and a ridge begins to form at the contact line. As solvent evaporation proceeds, the contact line remains pinned relative to the point O and the contact angle decreases as the solvent profile evolves from 1 to 3 as shown in figure 8(b). The ridge height, h_t, continues to grow due to the upward component of surface tension until this component gradually reduces with a decreasing drop height. When the etching depth is small, the solvent wetting conditions, apart from at the contact line, change little. The contact line receding may hardly be approached, or if at all possible, only endures for a short time period. That is to

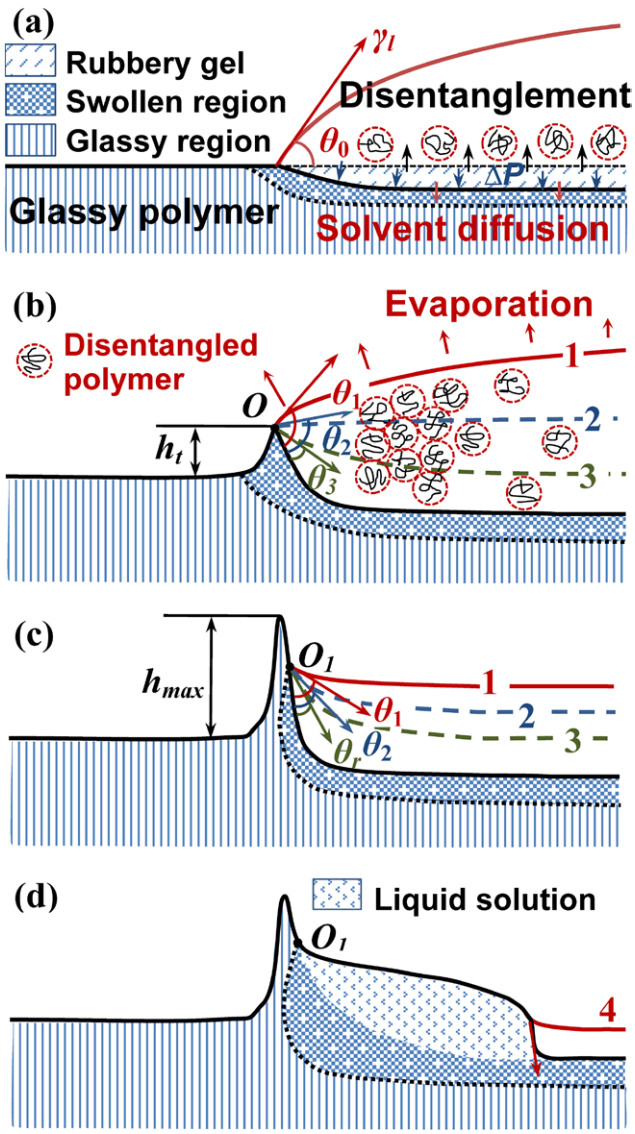

Figure 8. Wetting dynamics of the solvent drop with varying hole volumes when (a) and (b) the drop volume exceeds the via hole volume; (c) and (d) the via hole volume. outgrows the drop volume. Please note these illustrative sketches are not drawn to scale.

say, the transition from when there is an upward resolved surface tension component as at θ_1 to when there is a reversing downward resolved surface tension component as at θ_3 is less likely or can only last for a very short time. Even though there is a radial surface tension component dragging the softened polymer inward, the force is mainly exerted on the rim of the hole most of the time corresponding to a constant contact radius mode. It is believed this holds true for not only one drop, but also the first several drops, when the individual drop volume is much more than the volume of the via hole.

However, such wetting conditions cannot remain unchanged as both the ridge height and hole depth increase enlarging the hole volume as more drops are dispensed at the same location. The ridge height becomes approximately constant after the polymer thickness reaches a certain value, as confirmed by figure 9. This is attributed to a significant change in the wetting condition when the via hole volume outgrows the drop

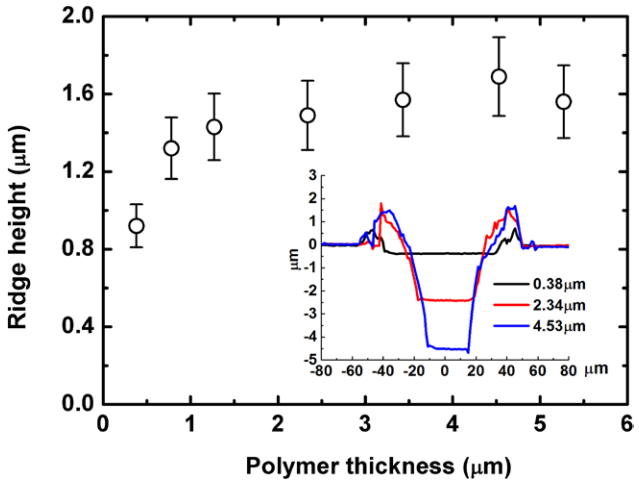

Figure 9. The measured ridge height for completely etched via holes versus the polymer thickness. The inset illustrates the superimposition of profiles of three completely etched via holes for varied polymer thicknesses.

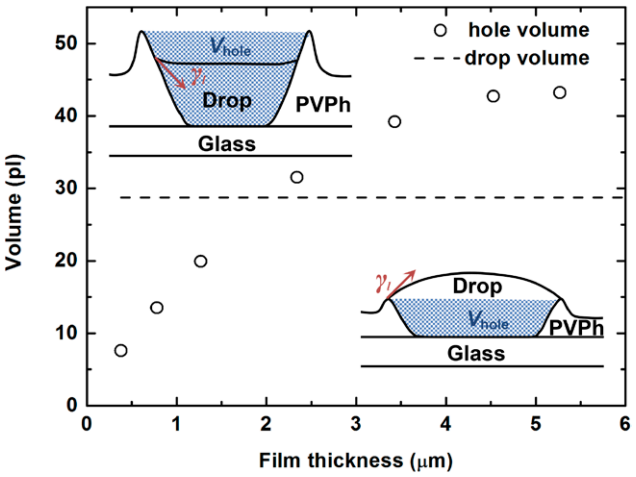

Figure 10. Transition of the drop wetting condition based on the relationship between drop volume and hole volume.

volume. The volume of the via hole can be satisfactorily estimated using a truncated cone approximation. To confirm this, a lower limit estimate of the via hole volume was calculated by summing the volumes of a number of discs each with a thickness of 0.1 μm locating within the hole. The deviation between this lower limit and the estimate using a truncated cone is usually less than 6%. In our experiment, the volume of the via hole exceeds that of the in-flight droplet when the polymer thickness is above 2 μm, as shown in figure 10. Therefore, any more drops dispensed are expected to locate within the via hole rather than wetting up to the rim at such polymer thicknesses, as indicated in figure 8(c). When such wetting conditions are established, the convex solvent profile (bottom right inset in figure 10) evolves to a more flat profile (top left inset in figure 10). As evaporation proceeds, the constant contact radius mode prevails so that the contact line is pinned at the point O_1, which is below the rim. The region far above O_1 is less prone to be deformed, while the polymer in the vicinity of the surface wetted by the receding contact line is still softened and can be pulled inward towards the centre. This induces a near-flat to a concave liquid–gas interface transition which in turn results in an even longer evaporation time. When the contact angle approaches the receding contact angle θ_r, the contact line starts receding following a constant contact angle mode. Simultaneously the dissolved polymer is re-deposited near the sidewall due to the coffee ring effect. Therefore, below O_1 the sidewall is prone to proceed to the centre of the hole accordingly, resulting in a narrower D_{in} and a steeper sidewall, as sketched in figure 8(d). This can also be observed in the profile superimposition in the inset of figure 9 with a more convex curve to the sidewall for thick layers. However, after several drops have been dispensed, the effect of the wetting dynamics as discussed in figure 8, results in a narrower bottom and a smaller D_{in} of a comparable order to H_d. This topography change leads to a non-negligible lateral etching of the sidewall and polymer dissolution into the solvent located within the via hole. When the drop is entrapped inside the via hole, as sketched in the top left inset in figure 10, and the evaporation time needed is longer than a sessile drop of the same volume, it allows longer time for the polymer to diffuse into the solvent. At this point, the process is diffusion dominant. Diffusion of the polymer into the entrapped solvent both laterally from the sidewall and vertically from the bottom causes a high polymer concentration and viscosity of the solution, weakening any further polymer diffusion. At the same time, the coffee ring flow cannot transfer the polymer anywhere away from the already cramped hole, which could result in substantial removal of polymer. Therefore the polymer will eventually refill the hole as the solvent evaporates.

6. Conclusions

The averaged flow velocity within an IPA sessile drop was calculated as a function of the distance from the sessile drop centre and contact angle based on lubrication theory. Calculations based on the height-averaged flow reveal that the inward diffusion of PVPh in IPA is weaker compared with the outward coffee ring flow during the initial stage, resulting in complete removal of the polymer from the central region. The interrelationship between the IPA drop volume and the resulting via hole volume drastically changes the wetting dynamics of IPA on PVPh. With the sessile drop wetting behaviour changing from wetting to the rim to being confined within the hole, any more polymer re-deposition needs to occur within the cramped space and the surface tension continues pulling the softened polymer inward, further contributing to the decrease of the inner diameter. During this later stage, non-negligible horizontal polymer dissolution from the sidewall, along with vertical polymer dissolution from the bottom cause a high polymer concentration within limited space. This inhibits further polymer etching and the via hole will get refilled eventually preventing from the polymer layer being further etched down. This increased understanding of the dynamics of this hole etching process will allow for further modelling work to estimate the penetration limit for different solvent/polymer systems, which is aimed for evaluation of using inkjet etching to fabricate holes for printed electronics applications and its limits.

Appendix

The integral function $v(r,t) = -\frac{1}{\rho r h}\int_0^r \left[J(r,t)\sqrt{1+\left(\frac{\partial h}{\partial r}\right)^2} + \rho\frac{\partial h}{\partial t}\right] r\mathrm{d}r$ can be split into two terms, v_1 and v_2:

$$v(r,t) = -\frac{1}{\rho r h}\int_0^r J(r,t)\sqrt{1+\left(\frac{\partial h}{\partial r}\right)^2}\, r\mathrm{d}r - \frac{1}{rh}\int_0^r \frac{\partial h}{\partial t} r\mathrm{d}r = v_1 + v_2, \tag{A.1}$$

where $v_1 = -\frac{1}{\rho r h}\int_0^r J(r,t)\sqrt{1+\left(\frac{\partial h}{\partial r}\right)^2}\, r\mathrm{d}r$ and $v_2 = -\frac{1}{rh}\int_0^r \frac{\partial h}{\partial t} r\mathrm{d}r$.

To calculate $v(r,t)$, both $J(r,t)$ and $h(r,t)$ need to be specified. The following explicit expressions of $J(r,t) = J_0(\theta)(1-\tilde{r}^2)^{-\lambda(\theta)}$,

$$J_0(\theta) = \frac{Dc_v}{R}(0.27\theta^2 + 1.30)[1-\Lambda(\theta)],$$

$$\Lambda(\theta) = \lambda(\theta) + \delta(\theta) = 0.2239\left(\theta - \frac{\pi}{4}\right)^2 + 0.3619,$$

$\lambda(\theta) = 0.5 - \frac{\theta}{\pi}$, $h(r,t) = \sqrt{\frac{R^2}{\sin^2\theta} - r^2} - \frac{R}{\tan\theta}$, and $\sqrt{1+\left(\frac{\partial h}{\partial r}\right)^2} = (1-\tilde{r}^2)^{-\delta(\theta)}$ are used here and are taken from Hu and Larson [49, 50], where $J_0(\theta)$ is the evaporation flux at $r = 0$ for a specific contact angle θ (kg m^{-2} s^{-2}); $\tilde{r} = r/R$; D is the diffusion coefficient of the solvent into air (m^2 s^{-1}); and c_v is the saturated vapour concentration (kg m^{-3}).

Therefore, we have:

$$\begin{aligned} v_1 &= -\frac{1}{\rho r h}\int_0^r J(r,t)\sqrt{1+\left(\frac{\partial h}{\partial r}\right)^2} r\mathrm{d}r \\ &= -\frac{1}{\rho r h}\int_0^r J_0(\theta)(1-\tilde{r}^2)^{-\lambda(\theta)}(1-\tilde{r}^2)^{-\delta(\theta)} r\mathrm{d}r \\ &= -\frac{1}{\rho r h}\int_0^r \frac{Dc_v}{R}(0.27\theta^2+1.30)[1-\Lambda(\theta)](1-\tilde{r}^2)^{-\Lambda(\theta)} r\mathrm{d}r \\ &= -\frac{RDc_v(0.27\theta^2+1.30)}{2\rho r h}[(1-r^2/R^2)^{1-\Lambda(\theta)} - 1]. \end{aligned} \tag{A.2}$$

According to Hu and Larson [50]:

$$\frac{\partial h}{\partial t} = \dot{h}(0,t)(1-\tilde{r}^2) = \frac{2\dot{m}(t)}{\rho\pi R^2}(1-\tilde{r}^2) \tag{A.3}$$

$$\dot{m}(t) = -\pi RDc_v(0.27\theta^2 + 1.30). \tag{A.4}$$

Substitution of equations (A.3) and (A.4) into v_2 yields:

$$\begin{aligned} v_2 &= -\frac{1}{rh}\int_0^r \frac{\partial h}{\partial t} r\mathrm{d}r \\ &= \frac{2}{rh}\int_0^r \frac{\pi RDc_v(0.27\theta^2+1.30)}{\rho\pi R^2}(1-\tilde{r}^2) r\mathrm{d}r \\ &= -\frac{RDc_v(0.27\theta^2+1.30)}{\rho r h}\int_0^{\mathrm{r}} (1-\tilde{r}^2)\mathrm{d}(1-\tilde{r}^2) \\ &= -\frac{RDc_v(0.27\theta^2+1.30)}{2\rho r h}\left[\left(1-\frac{r^2}{R^2}\right)^2 - 1\right]. \end{aligned} \tag{A.5}$$

Hence, equation (A.1) can be expressed as:

$$\begin{aligned} v(r,t) &= v(r,\theta) \\ &= -\frac{RDc_v(0.27\theta^2+1.30)}{2\rho r\sqrt{\frac{R^2}{\sin^2\theta} - r^2} - \frac{R}{\tan\theta}}\left[\left(1-\frac{r^2}{R^2}\right)^{0.6381 - 0.2239\left(\theta-\frac{\pi}{4}\right)^2} - 1\right] \\ &\quad - \frac{RDc_v(0.27\theta^2+1.30)}{2\rho r\sqrt{\frac{R^2}{\sin^2\theta} - r^2} - \frac{R}{\tan\theta}}\left[\left(1-\frac{r^2}{R^2}\right)^2 - 1\right]. \end{aligned} \tag{A.6}$$

The next step is to consider the diffusion of the polymer into the solvent. The diffusion length, which characterizes the propagation distance of the polymer concentration front in 1D, can be expressed as $L = 2\sqrt{D't}$, where D' is the polymer diffusivity in the solvent and t is the diffusion time. The diffusion coefficient D' can be estimated by $D' = k_B T/(6\pi\mu R_0)$, where k_B is the Boltzmann constant, T is temperature, μ is viscosity, and R_0 is the solute molecular radius [60]. If we use the radius of gyration $r_g = r_{rms}/\sqrt{6} = n^{\frac{1}{2}}l/\sqrt{6}$ as R_0, where r_{rms} is the root-mean-square length of an unperturbed randomly coiled polymer chain, n is the degree of polymerization and l is 1D link of length in the single freely joined chain model [48], then the diffusion length L can be expanded into: $L = \sqrt{4k_BTt/(6\pi\mu R_0)} = 2\sqrt{k_BTt/(\pi\mu l\sqrt{6n})}$. Taking the first order derivative of L yields:

$$v_d = \mathrm{d}L/\mathrm{d}t = \sqrt{k_BT/(\sqrt{6n}\,\pi\mu l t)} \tag{A.7}$$

References

[1] Chiolerio A and Sangermano M 2012 *In situ* synthesis of Ag-acrylic nanocomposites: tomography-based percolation model, irreversible photoinduced electromigration and reversible electromigration *Mater. Sci. Eng.* B **177** 373–80

[2] Giardi R, Porro S, Chiolerio A, Celasco E and Sangermano M 2013 Inkjet printed acrylic formulations based on UV-reduced graphene oxide nanocomposites *J. Mater. Sci.* **48** 1249–55

[3] Chiolerio A, Roppolo I and Sangermano M 2013 Radical diffusion engineering: tailored nanocomposite materials for piezoresistive inkjet printed strain measurement *RSC Adv.* **3** 3446–52

[4] Camarchia V, Chiolerio A, Cotto M, Fang J, Ghione G, Pandolfi P, Pirola M, Quaglia R and Ramella C 2014 Demonstration of inkjet-printed silver nanoparticle microstrip lines on alumina for RF power modules *Org. Electron.* **15** 91–8

[5] Marjanović N, Chiolerio A, Kus M, Ozel F, Tilki S, Ivanović N, Rakočević Z, Andrić V, Barudžija T and Baumann R R 2014 Magnetite nanoparticles: synthesis, thin film properties and inkjet printing of magnetic cores for inductor applications *Thin Solid Films* **570** 38–44

[6] Chiolerio A, Bocchini S and Porro S 2014 Inkjet printed negative supercapacitors: synthesis of polyaniline-based inks, doping agent effect, and advanced electronic devices applications *Adv. Funct. Mater.* **24** 3375–83

[7] Woo K, Kim D, Kim J S, Lim S and Moon J 2008 Ink-jet printing of Cu–Ag-based highly conductive tracks on a transparent substrate *Langmuir* **25** 429–33

[8] Kawase T, Shimoda T, Newsome C, Sirringhaus H and Friend R H 2003 Inkjet printing of polymer thin film transistors *Thin Solid Films* **438–439** 279–87

[9] Lim J A, Lee W H, Kwak D H and Cho K 2009 Evaporation-induced self-organization of inkjet-printed organic semiconductors on surface-modified dielectrics for high-performance organic transistors *Langmuir* **25** 5404–10

[10] Hebner T R, Wu C C, Marcy D, Lu M H and Sturm J C 1998 Ink-jet printing of doped polymers for organic light emitting devices *Appl. Phys. Lett.* **72** 519–21

[11] Kim D, Jeong S, Park B K and Moon J 2006 Direct writing of silver conductive patterns: improvement of film morphology and conductance by controlling solvent compositions *Appl. Phys. Lett.* **89** 264101

[12] de Gans B J, Hoeppener S and Schubert U S 2006 Polymer-relief microstructures by inkjet etching *Adv. Mater.* **18** 910–14

[13] de Gans B J, Hoeppener S and Schubert U S 2007 Polymer relief microstructures by inkjet etching *J. Mater. Chem.* **17** 3045–50

[14] Grimaldi I A, De Girolamo Del Mauro A, Nenna G, Loffredo F, Minarini C and Villani F 2011 Microstructuring of polymer films by inkjet etching *J. Appl. Polym. Sci.* **122** 3637–43

[15] Li G F, Graf K, Bonaccurso E, Golovko D S, Best A and Butt H J 2007 Evaporation structures of solvent drops evaporating from polymer surfaces: influence of molar mass *Macromol. Chem. Phys.* **208** 2134–44

[16] Chiolerio A, Rivolo P, Porro S, Stassi S, Ricciardi S, Mandracci P, Canavese G, Bejtka K and Pirri C F 2014 Inkjet-printed PEDOT:PSS electrodes on plasma-modified PDMS nanocomposites: quantifying plasma treatment hardness *RSC Adv.* **4** 51477–85

[17] Bonaccurso E, Butt H J, Hankeln B, Niesenhaus B and Graf K 2005 Fabrication of microvessels and microlenses from polymers by solvent droplets *Appl. Phys. Lett.* **86** 124101

[18] Pericet-Camara R, Best A, Nett S K, Gutmann J S and Bonaccurso E 2007 Arrays of microlenses with variable focal lengths fabricated by restructuring polymer surfaces with an ink-jet device *Opt. Express* **15** 9877–82

[19] Xia Y J and Friend R H 2007 Nonlithographic patterning through inkjet printing via holes *Appl. Phys. Lett.* **90** 253513

[20] Xia Y J and Friend R H 2006 Polymer bilayer structure via inkjet printing *Appl. Phys. Lett.* **88** 163508

[21] Lu J-P, Chen F-C and Lee Y-Z 2009 Ring-edged bank array made by inkjet printing for color filters *J. Disp. Technol.* **5** 162–5

[22] Kawase T, Sirringhaus H, Friend R H and Shimoda T 2001 inkjet printed via-hole interconnections and resistors for all-polymer transistor circuits *Adv. Mater.* **13** 1601–5

[23] Sirringhaus H, Kawase T, Friend R H, Shimoda T, Inbasekaran M, Wu W and Woo E P 2000 High-resolution inkjet printing of all-polymer transistor circuits *Science* **290** 2123–6

[24] Lennon A J, Ho-Baillie A W Y and Wenham S R 2009 Direct patterned etching of silicon dioxide and silicon nitride dielectric layers by inkjet printing *Sol. Energy Mater. Sol. Cells* **93** 1865–74

[25] Lennon A J, Utama R Y, Lenio M A T, Ho-Baillie A W Y, Kuepper N B and Wenham S R 2008 Forming openings to semiconductor layers of silicon solar cells by inkjet printing *Sol. Energy Mater. Sol. Cells* **92** 1410–15

[26] Yang Y S, You I-K, Koo J B, Lee S S, Lim S C and Youl K S 2010 Characteristics of via-hole interconnections fabricated by using an inkjet printing method *J. Korean Phys. Soc.* **57** 1699–701

[27] Yang Y S, Koo J B and You I-K 2012 Organic nonvolatile memory devices fabricated by using an inkjet printing method *J. Korean Phys. Soc.* **60** 1504–7

[28] Zhang Y, Liu C and Whalley D C 2012 The effect of droplet ejection frequency on the dimensions of inkjet-etched micro-via holes in poly4(-vinyl phenol) thin films *J. Phys. D: Appl. Phys.* **45** 125303

[29] Zhang Y, Liu C and Whalley D C 2012 The penetration limit of poly(4-vinyl phenol) thin films for etching via holes by inkjet printing *Appl. Phys. Lett.* **101** 253302

[30] Reis N, Ainsley C and Derby B 2005 Ink-jet delivery of particle suspensions by piezoelectric droplet ejectors *J. Appl. Phys.* **97** 094903

[31] Wijshoff H 2010 The dynamics of the piezo inkjet printhead operation *Phys. Rep.* **491** 77–177

[32] Martin G D, Hoath S D and Hutchings I M 2008 Inkjet printing—the physics of manipulating liquid jets and drops *J. Phys.: Conf. Ser.* **105** 012001

[33] Schönfeld F, Graf K, Hardt S and Butt H J 2008 Evaporation dynamics of sessile liquid drops in still air with constant contact radius *Int. J. Heat Mass Transfer* **51** 3696–9

[34] Dong H, Carr W W and Morris J F 2006 Visualization of drop-on-demand inkjet: drop formation and deposition *Rev. Sci. Instrum.* **77** 085101

[35] 2012 *Inkjet-Based Micromanufacturing* (Wiley-VCH)

[36] Park J-U *et al* 2007 High-resolution electrohydrodynamic jetting printing *Nat. Mater.* **6** 782–9

[37] Mishra S, Barton K L, Alleyne A G, Ferreira P M and Rogers J A 2010 High-speed and drop-on-demand printing with a pulsed electrohydrodynamic jet *J. Micromech. Microeng.* **20** 095026

[38] Park J-U, Lee S, Unarunotai S, Sun Y, Dunham S, Song T, Ferreira P M, Alleyene A G, Paik U and Rogers J A 2010 Nanoscale, electrified liquid jets for high-resolution printing of charge *Nano Lett.* **10** 584–91

[39] Teng L, Plötner M, Türke A, Adolphi B, Finn A, Kirchner R and Fischer W-J 2013 Nanoimprint assisted inkjet printing to fabricate sub-micron channel organic field effect transistors *Microelectron. Eng.* **110** 292–7

[40] Ko S H, Pan H, Grigoropoulos C P, Fréchet J M J, Luscombe C K and Poulikakos D 2008 Lithography-free high-resolution organic transistor arrays on polymer substrate by low energy selective laser ablation of inkjet-printed nanoparticle film *Appl. Phys.* A **92** 579–87

[41] Yokota T, Sekitani T, Kato Y, Kuribara K, Zschieschang U, Klauk H, Yamamoto T, Takimiya K, Kuwabara H, Ikeda M and Someya T 2011 Low-voltage organic transistor with subfemtoliter inkjet source–drain contacts *MRS Commun.* **1** 3–6

[42] Yokota T, Kuribara K, Tokuhara T, Zschieschang U, Klauk H, Takimiya K, Sadamitsu Y, Hamada M, Sekitani T and Someya T 2013 Flexible low-voltage organic transistors with high thermal stability at 250 °C *Adv. Mater.* **25** 3639–44

[43] Deegan R D 2000 Pattern formation in drying drops *Phys. Rev.* E **61** 475–85

[44] Deegan R D, Bakajin O, Dupont T F, Huber G, Nagel S R and Witten T A, 1997 Capillary flow as the cause of ring stains from dried liquid drops *Nature* **389** 827–9

[45] Deegan R D, Bakajin O, Dupont T F, Huber G, Nagel S R and Witten T A 2000 Contact line deposits in an evaporating drop *Phys. Rev.* E **62** 756–65

[46] Derby B 2010 Inkjet printing of functional and structural materials: fluid property requirements, feature stability, and resolution *Annu. Rev. Mater. Res.* **40** 395–414

[47] Reid R C, Prausnitz J M and Poling B E 1987 *The Properties of Gases and Liquids* 4th edn (New York: McGraw-Hill) p 741

[48] Bower D I 2002 *An Introduction to Polymer Physics* (Cambridge: Cambridge University Press)
[49] Hu H and Larson R G 2002 Evaporation of a sessile droplet on a substrate *J. Phys. Chem.* B **106** 1334–44
[50] Hu H and Larson R G 2005 Analysis of the microfluid flow in an evaporating sessile droplet *Langmuir* **21** 3963–71
[51] Lapointe F, Pézolet M and Brisson J 2007 Orientation relaxation study on poly(ethylene oxide)-poly(vinyl phenol) blends by polarization modulation infared linear dichroism *Polymer* **48** 5626–38
[52] Pericet-Camara R, Auernhammer G K, Koynov K, Lorenzoni S, Raiteri R and Bonaccurso E 2009 Solid-supported thin elastomer films deformed by microdrops *Soft Matter*. **5** 3611–17
[53] Rusanov A I 1975 *Colloid J. USSR* **37** 614–22
[54] Mao T, Kuhn D C S and Tran H 1997 Spread and rebound of liquid droplets upon impact on flat surfaces *AIChE J.* **43** 2169–79
[55] Desie G, Allaman S, Lievens O, Anthonidssen K and Soucemarianadin A 2002 Influence of substrate properties in drop on demand printing *Int. Conf. on Digital Printing Technologies*
[56] Miller-Chou B A and Koenig J L 2003 A review of polymer dissolution *Prog. Polym. Sci.* **28** 1223–70
[57] Pericet-Camara R, Bonaccurso E and Graf K 2008 Microstructuring of polystyrene surfaces with nonsolvent sessile droplets *Chem. Phys. Chem.* **9** 1738–46
[58] Fredrickson G H, Ajdari A, Leibler L and Carton J P 1992 Surface modes and deformation energy of a molten polymer brush *Macromolecules* **25** 2882–9
[59] Long D, Ajdari A and Leibler L 1996 Static and dynamic wetting properties of thin rubber films *Langmuir* **12** 5221–30
[60] Cussler E L 2009 *Diffusion Mass Transfer in Fluid Systems* (Cambridge: Cambridge University Press)